

# Doping profile engineered triple heterojunction TFETs with 12 nm body thickness

Chin-Yi Chen, Hsin-Ying Tseng, Hesameddin Ilatikhameneh, Tarek A. Ameen, Gerhard Klimeck,

Mark J. Rodwell, Michael Povolotskyi

**Abstract**—Triple heterojunction (THJ) TFETs have been proposed to resolve the low ON-current challenge of TFETs. However, the design space for THJ-TFETs is limited by fabrication challenges with respect to device dimensions and material interfaces. This work shows that the original THJ-TFET design with 12 nm body thickness has poor performance, because its sub-threshold swing is 50 mV/dec and the ON-current is only  $6 \mu\text{A}/\mu\text{m}$ . To improve the performance, the doping profile of THJ-TFET is engineered to boost the resonant tunneling efficiency. The proposed THJ-TFET design shows a sub-threshold swing of 40 mV/dec over four orders of drain current and an ON-current of  $325 \mu\text{A}/\mu\text{m}$  with  $V_{GS} = 0.3 \text{ V}$ . Since THJ-TFETs have multiple quantum wells and material interfaces in the tunneling junction, quantum transport simulations in such devices are complicated. State-of-the-art mode-space quantum transport simulation, including the effect of thermalization and scattering, is employed in this work to optimize THJ-TFET design.

**Index Terms**—tunnel field effect transistors, triple heterojunction TFETs, channel thickness, atomistic mode-space quantum transport, scattering

## I. INTRODUCTION

Power consumption in CPUs has impacted Moore's law significantly [1], [2]. An obvious solution to reduce the power supply is to replace the metal-oxide-semiconductor field-effect transistors (MOSFETs), which is limited by the Boltzmann tyranny, with new devices like the tunneling field-effect transistors (TFETs) [3]–[12] and negative-capacitance field-effect transistors (NC-FETs) [13], [14]. However, these steep sub-threshold slope devices come with challenges that hinder their wide-spread applications. The primary challenge of TFETs is its low ON-current. TFETs are shown to suffer from low ON-current issue since the quantum tunneling probability is usually much lower than one [15].

The tunneling probability depends on several factors, such as tunneling distance, electric field, resonance conditions, and effective tunneling mass. Several approaches have been introduced to increase the tunneling probability based on

This was supported by National Science Foundation E2CDA Type I collaborative research on "A Fast 70mV Transistor Technology for Ultra-Low-Energy Computing" with the award number of 1639958 and semiconductor research corporation with its task ID of 2694.003. The use of nanoHUB.org computational resources operated by the Network for Computational Nanotechnology funded by the US National Science Foundation under Grant Nos. EEC-1227110, EEC-0228390, EEC-0634750, OCI-0438246, and OCI-0721680 is gratefully acknowledged. NEMO5 developments were critically supported by an NSF Peta-Apps award OCI-0749140 and by Intel Corp. This work also used the Extreme Science and Engineering Discovery Environment (XSEDE) at SDSC Dell Cluster with Intel Haswell Processors (Comet) through 50,000.0 SUs under charge number TG-ECS190009.

The authors are with the Department of Electrical and Computer Engineering, Purdue University, West Lafayette, IN, 47907 USA e-mail: r99941001@gmail.com

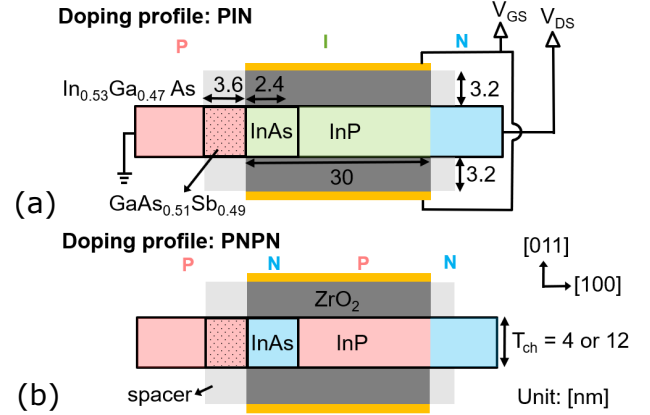


**Fig. 1:** Device design of a triple heterojunction TFET with (a) conventional doping profile (PIN) and (b) an optimized doping profile (PNPN).

optimizing these four factors. For example, in GaN-based heterojunction TFETs, the tunneling distance is reduced by engineering the band-diagram [16]; in a dielectric engineered TFET, the electric field at the tunneling junction is increased by using two different dielectrics [17]; in a resonance-TFET, quantum resonances are used to increase the tunneling probability close to one [18]; in a Phosphorene-based TFET, the low effective tunneling mass increases the tunneling probability [19].

A triple heterojunction (THJ-) TFET based on III-V materials allows an advantage in optimizing all of the factors mentioned above. A triple heterojunction reduces the tunneling distance using the band diagram engineering. It also uses resonance tunneling to improve the tunneling probability in the ON-state and provides small effective tunneling mass due to III-V materials [20]–[23].

Despite the benefits of THJ-TFETs, the fabrication constraints, such as device dimensions and material combinations, limit the performance of a THJ-TFET. For example, a 4 nm thick THJ-TFET with a conventional PIN doping profile shown in Fig. 1(a) predicts an excellent performance; however, as the body thickness ( $T_{ch}$ ) approaches a realistic value of 12 nm, the performance degrades.

The reason for the high sensitivity of performance on body thickness in the original design is that, in PIN structures, the electric field ( $E$ ) at the tunnel junction depends on both the depletion width ( $W_D$ ) and the scaling length ( $\lambda$ ), as shown in Eq. 1 [24], [25]:

$$E \propto 1/(W_D + \lambda(T_{ch})) \quad (1)$$

To address these issues in designing THJ-TFETs, the doping profile is engineered, as shown in Fig. 1(b). By replacing

the intrinsic part of the channel with the doped regions, the electric field is determined by the depletion width, which is not strongly dependent on  $T_{ch}$  as shown in Eq. 2.

$$E \propto 1/(W_{D,source} + W_{D,channel}) \quad (2)$$

Hence, the proposed design provides better performance for thicker devices by reducing the impact of thickness on the electrostatic profile.

The proposed design also considers fabrication technology constraints, including the limitation of the doping density in each material, the width of the strained quantum well, the crystal growth direction, and the channel material's choice to have a high-quality oxide interface. The proposed design shows the sub-threshold swing of 40 mV/dec over four orders of drain current. The high ON-current of 325  $\mu\text{A}/\mu\text{m}$  is achieved with a low supply voltage ( $V_{DD}$ ) of 0.3 V.

The device design optimization is performed using the Nanoelectronics Modeling tool NEMO5 [26], [27]. The atomistic tight-binding method with a ten orbital  $sp^3d^5s^*$  basis is used [28]. Carrier transport in THJ-TFETs is complex due to the presence of quantum wells in the tunneling region. The non-equilibrium quantum mechanics of the system includes the electron-electron scattering and electron-phonon scattering of carriers in these quantum wells, tunneling process at multiple interfaces, and quantum confinement effects [29]–[36]. To capture these mechanisms, atomistic quantum transport simulation, including effective thermalization [37], [38], is necessary to evaluate the device performance. Since a real-space atomistic simulation is computationally challenging for devices with a large dimension, the atomistic mode-space approach developed in Ref. [39] is applied in this work.

The paper is divided in four sections. The THJ-TFET device structure, that satisfies fabrication constraints, is presented in section II. The design principles for the THJ-TFET with the body thickness of 12 nm are discussed in section III. In section IV, we demonstrate the performance of the proposed THJ-TFET. And, the impact of the channel doping density is further discussed in section V.

## II. THJ-TFET DEVICE STRUCTURE

Fig. 1 shows the double-gated ultra-thin-body (UTB) THJ-TFET studied in this work. Fig. 1(a) is the THJ-TFET with a conventional PIN doping profile. It consists of a P-doped source, an intrinsic channel, and an N-doped drain. In the P-doped source,  $\text{In}_{0.53}\text{Ga}_{0.47}\text{As}$  and  $\text{GaAs}_{0.51}\text{Sb}_{0.49}$  have the doping density of  $N_a = 5 \times 10^{19} \text{ cm}^{-3}$ . InAs and InP channel are intrinsic. In the N-doped drain, InP has the doping density of  $N_d = 2 \times 10^{19} \text{ cm}^{-3}$ .

The UTB confinement direction is along  $\langle 011 \rangle$  crystal direction and the electron transport direction is along  $\langle 100 \rangle$  crystal direction. The electron transport direction is the same as the crystal growth direction to simulate the device structure fabricated by the vertical Fin-TFET technology [40]. The choice of the materials in the heterojunction is compatible with current crystal growth technology limitations. The substrate is assumed to be InP such that InAs quantum well is under 3.41% bi-axial compressive strain, while  $\text{In}_{0.53}\text{Ga}_{0.47}\text{As}$  and  $\text{GaAs}_{0.51}\text{Sb}_{0.49}$  are not strained since they are lattice-matched to InP substrate. The technology of growing  $\text{In}_{0.53}\text{Ga}_{0.47}\text{As}$ ,

$\text{GaAs}_{0.51}\text{Sb}_{0.49}$ , and InAs on InP(100) substrate through molecular beam epitaxy (MBE) are all well-developed [41]–[43]. The width of  $\text{GaAs}_{0.51}\text{Sb}_{0.49}$  source quantum well is 3.6 nm. The width of strained InAs channel quantum well is 2.4 nm, which is less than the critical thickness of 4 nm [44], [45]. The gate length is 30 nm, and the oxide thickness is 3.2 nm. The oxide material is assumed to be  $\text{ZrO}_2$  with a relative dielectric constant of 15. The source is grounded. The drain is under the applied supply voltage ( $V_{DD} = 0.3 \text{ V}$ ). The source to drain bias ( $V_{DS}$ ) is 0.3 V. The spacer in this work is assumed to be air with the dielectric constant of 1.

Fig. 1(b) is the proposed design with the same device structure as Fig. 1(a) while the doping is changed to the PNP doping profile. In the optimized PNP doping profile, the InAs channel quantum well is doped to N-type with  $N_d = 2 \times 10^{19} \text{ cm}^{-3}$ . The InP channel is doped to P-type with  $N_a = 2 \times 10^{19} \text{ cm}^{-3}$ .

## III. ORIGINAL THJ-TFET DESIGN PRINCIPLES

The design principle of the original THJ-TFETs is introduced in this section before describing the new design, PNP-doped THJ-TFET. The energy-resolved local density of states (LDOS) and transmission probability for the original THJ-TFET with different body thicknesses ( $T_{ch}$ ) are shown in Fig. 2. The doping profile is a conventional PIN doping profile shown in Fig. 1(a). The LDOS in Fig. 2 is calculated when the device is operated in the ON-state, where the gate to source bias ( $V_{GS}$ ) is 0.3 V. In Fig. 2(a), the alignment of the resonant states in the GaAsSb and InAs quantum wells results in the enhanced resonant tunneling such that the transmission probability is close to 1. On the other hand, in Fig. 2(b), when the body thickness increases to 12 nm, the resonant states are not aligned due to the worse gate control. The transmission, therefore, reduces 1~2 orders compared to the case of 4 nm body thickness.

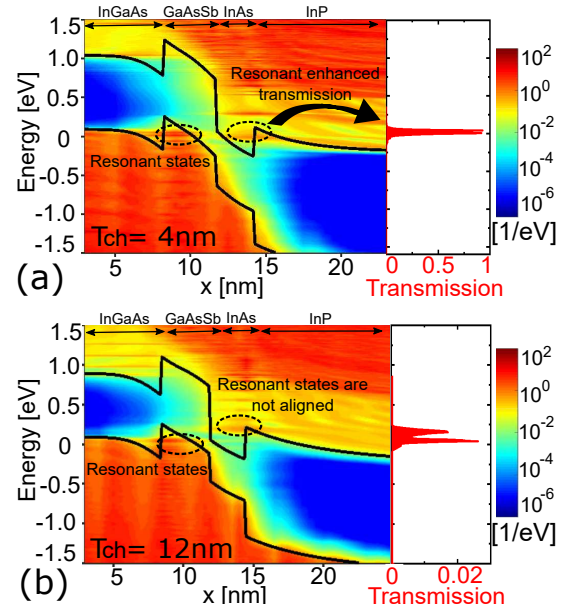


**Fig. 2:** Original THJ-TFET design principle: alignment of resonant states. (a) and (b) are the energy-resolved local density of states and transmission for 4 nm and 12 nm thick THJ-TFET when the device is operated in the ON-state.

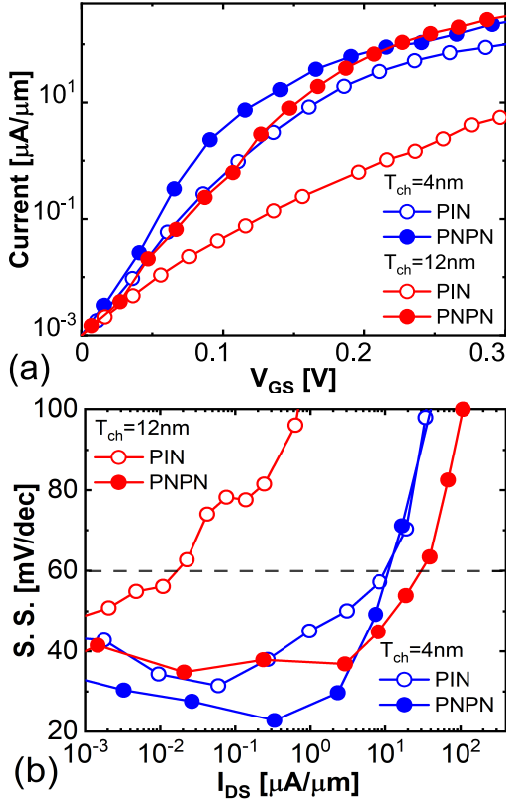


**Fig. 3:** (a) Transfer IV characteristics and (b) the S.S. -  $I_{DS}$  curve of a triple heterojunction TFET with a conventional doping profile (PIN) and the optimized doping profile (PNPN) for different body thicknesses ( $T_{ch}$ ) of 4 nm and 12 nm.

The key design rule of THJ-TFETs is to align the resonant states of two quantum wells in the tunneling junction and to introduce the resonant enhanced transmission. In the next section, the performance of 12 nm thick THJ-TFET is improved by aligning the resonant states through the proposed PNP doping profile shown in Fig. 1(b).

#### IV. IMPROVED THJ-TFET WITH PNP DOPING PROFILE

In this section, the performance of THJ-TFET with the PNP doping profile is demonstrated. The PNP doping profile was originally proposed for homojunction TFETs to improve electric field in the tunneling region [46]–[49]. It plays a more significant role in THJ-TFETs with thick body thickness. The PNP doping profile can be engineered in THJ-TFETs not only to increase the electric field, but also to help aligning the resonant states that introduces the resonance tunneling.

Fig. 3(a) compares the transfer characteristics of THJ-TFETs with 4 nm and 12 nm body thicknesses for different doping profiles. The gate to source bias ( $V_{GS}$ ) are shifted to have a fixed OFF-current value of  $10^{-3} \mu\text{A}/\mu\text{m}$  at  $V_{GS} = 0$  V. For THJ-TFET with the PIN doping profile, when the body thickness increases from 4 nm to 12 nm, the loss of gate control dominates the performance such that the ON-current ( $I_{ON}$ ) decreases by a factor of  $\sim 16$ .

However, for the THJ-TFET with the optimized PNP doping profile, the same thickness increment is shown to improve the ON-current by  $\sim 30\%$ . The reason is that, when the body

thickness increases from 4 nm to 12 nm, the engineered built-in electric field in tunneling junction alleviates the effect of gate control degradation by a better doping profile design. At the same time, the decrease of the confined materials' bandgaps ( $E_g$ ) enhances the ON-current [25]. The bandgaps of the materials used in the heterojunctions for different body thicknesses are listed in TABLE I. The ON-current of the THJ-TFET with different body thicknesses and the doping profiles is summarized in TABLE II.

The sub-threshold swing (S.S.)- $I_{DS}$  curve for the THJ-TFETs with the PIN doping profile and the optimized PNP doping profile for 4 nm and 12 nm thick THJ-TFETs are demonstrated in Fig. 3(b). For a body thickness of 4 nm, the sub-threshold swing for the conventional PIN doping profile and the optimized PNP doping profile does not show a significant difference. Both doping profiles exhibit decent performance. However, as the body thickness increases to 12 nm, the optimized PNP doping profile retains its high performance, whereas the conventional PIN doping profile degrades drastically.

To further understand why THJ-TFET with the optimized PNP doping profile has a better performance comparing to the case of the traditional PIN doping profile, the local density of states (LDOS) at  $V_{GS} = 0.3$  V for different body thicknesses and different doping profiles are shown in Fig. 4.

When the channel thickness of the PIN-doped THJ-TFET increases from 4 nm to 12 nm, the quantum well states are misaligned, as shown in Fig. 4(a) and (c). The resonant states in the InAs channel quantum well are outside the tunneling window. The lack of resonance tunneling leads to significant degradation of the transmission probability and the ON-current. On the other hand, the optimized PNP doping profile helps to retain the alignment of GaAsSb and InAs quantum well states in the 12 nm thick THJ-TFET, as shown in Fig. 4(d). The performance of 12 nm thick THJ-TFETs with the optimized PNP doping profile is, therefore, similar to the case of a thinner channel thickness.

The tunneling distance is determined by the electric field in TFET's tunneling region. Generally, the tunneling distance of a TFET with a conventional PIN doping profile is highly sensitive to the body thickness; a thinner device has a stronger gate control that leads to a smaller natural scaling length and hence a smaller tunneling distance [39], [50], [51]. Since the device with an optimized PNP doping profile has no intrinsic region in the channel, the scaling lengths are dominated by the depletion width corresponding to the doping profile [51]. As a result, the optimized PNP doping profile is not just engineered to increase the electric field in the tunneling

$T_{ch}$		InGaAs	GaAsSb	InAs	GaAsSb
4 nm	$E_g$ [eV]	0.9517	0.9871	0.7016	1.504
	$\Delta E_v$ [eV]	0	0.4238	0.0456	-0.3796
12 nm	$E_g$ [eV]	0.7993	0.8456	0.5010	1.3822
	$\Delta E_v$ [eV]	0	0.4273	0.0670	-0.3902

**TABLE I:** The confined bandgap ( $E_g$ ) and valence band off-set ( $\Delta E_v$ ) of the heterojunction materials used in the design. The UTB's confinement direction is along  $\langle 110 \rangle$ . The atomistic tight-binding parameters used in this work are from [28].

$T_{ch}$	4 nm	12 nm	4 nm	12nm
Doping profile	(PIN)	(PIN)	(PNPN)	(PNPN)
$I_{ON}$ [ $\mu A/\mu m$ ]	98	6	248	325

**TABLE II:** The ON-current ( $I_{ON}$ ) of the triple heterojunction TFET with body thicknesses of 4 nm and 12nm for both conventional PIN doping profile and the PNPN doping profile. The  $I_{ON}$  is extracted at  $V_{GS} = 0.3V$ .

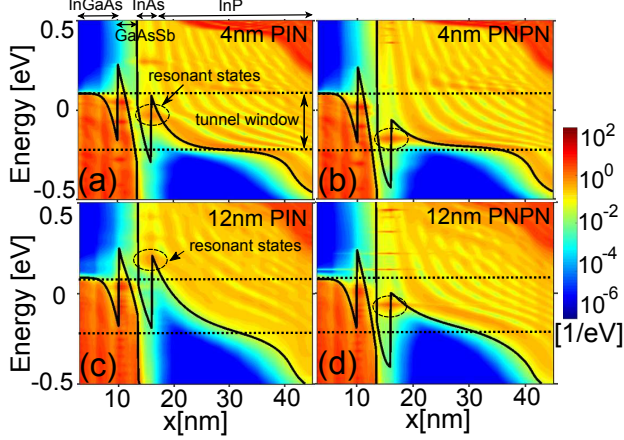


**Fig. 4:** Local density of states (LDOS) of the triple heterojunction TFETs with the body thickness/doping profile of (a) 4 nm / PIN, (b) 4 nm / PNPN, (c) 12 nm / PIN, and (d) 12 nm / PNPN. LDOS is calculated in the ON-state where  $V_{GS} = 0.3 V$ .

junction; it also reduces the sensitivity of the performance to the body thickness. Fig. 5 shows the impact of doping profile and body thickness on the electric field along the channel. The peak electric field in PNPN doped THJ-TFETs has less dependence on the body thickness compared to the conventional PIN doped THJ-TFETs.

### V. P-DOPED INP CHANNEL DOPING DENSITY

The benefit of having a P-N junction in the tunneling region is intuitive and is well-studied [46]–[49]. The electric field in the tunneling region is enhanced by P-N junction's built-in

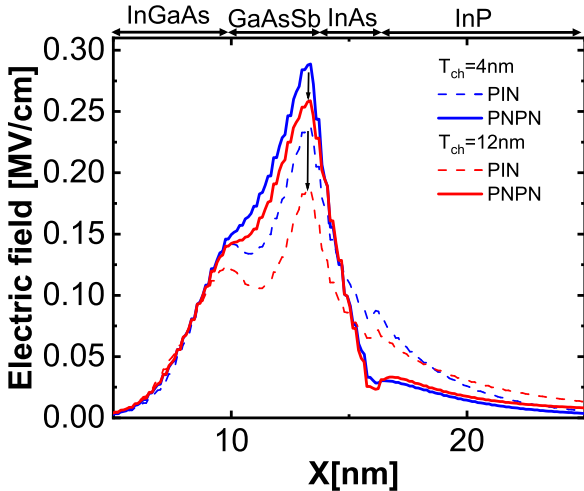


**Fig. 5:** Electric field along the channel for 4 nm and 12 nm thick triple heterojunction TFETs with both conventional PIN doping profile and optimized PNPN doping profile. The electric field is obtained for the ON-state with  $V_{GS} = 0.3 V$ .

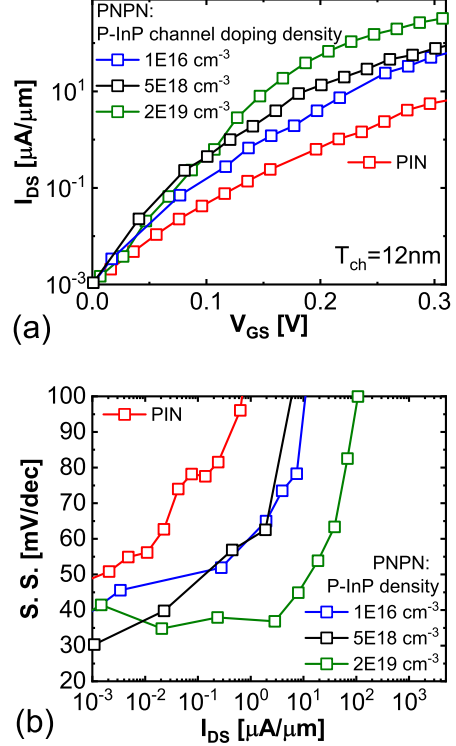


**Fig. 6:** (a) Transfer IV characteristics and (b) S.S. -  $I_{DS}$  curve of the 12 nm thick triple heterojunction TFETs with the PIN and PNPN doping profile. The PNPN-doped TFETs with different P-InP channel doping densities are demonstrated.

potential and therefore leads to a smaller tunneling distance and a larger transmission probability. The design rule of the P-N junction in the tunneling region is to maximize the doping density to achieve the maximum built-in potential. However, the role of the P-doped channel in the PNPN-doped THJ-TFET is not yet well understood. In this section, the doping density of the P-doped InP channel is studied.

The transfer characteristics and S.S. -  $I_{DS}$  curve of PNPN-doped THJ-TFET with different P-InP channel doping density are shown in Fig. 6. The body thickness of the device is 12 nm. The ON-current at  $V_{GS} = 0.3 V$  is summarized in TABLE III. The PNPN-doped THJ-TFET with P-InP channel doping density of  $1 \times 10^{16} cm^{-3}$  is the reference case to observe the improvement from applying the P-N junction in the tunneling region. The ON-current increases from  $6 \mu A/\mu m$  to  $50 \mu A/\mu m$  when the doping profile is replaced from PIN doping profile to PNPN doping profile with P-InP channel doping density of  $1 \times 10^{16} cm^{-3}$ .

Interestingly, the performance of 12 nm thick THJ-TFET improves slightly when P-InP channel doping density increases from  $1 \times 10^{16} cm^{-3}$  to  $5 \times 10^{18} cm^{-3}$ . The ON-current increases from  $50 \mu A/\mu m$  to  $78 \mu A/\mu m$ . The case with InP

Doping profile	PIN	PNPN	PNPN	PNPN
P-InP channel doping	-	$1 \times 10^{16}$	$5 \times 10^{18}$	$2 \times 10^{19}$
$I_{ON}$ [ $\mu A/\mu m$ ]	6	50	78	325

**TABLE III:**  $I_{ON}$  at  $V_{GS} = 0.3 V$  of the 12 nm thick THJ-TFET with different doping profiles, such as conventional PIN doping profile and the PNPN doping profile, are listed.

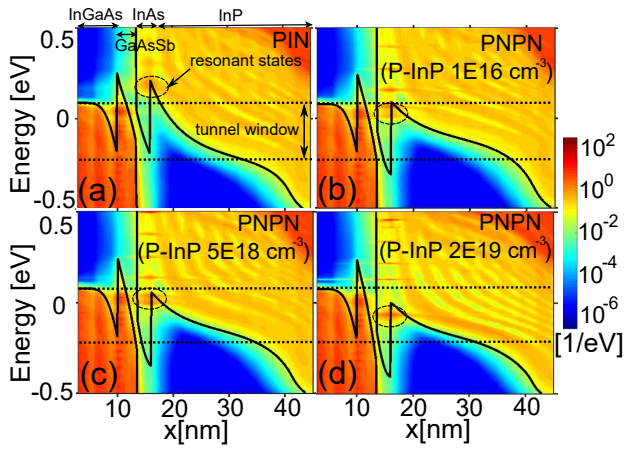


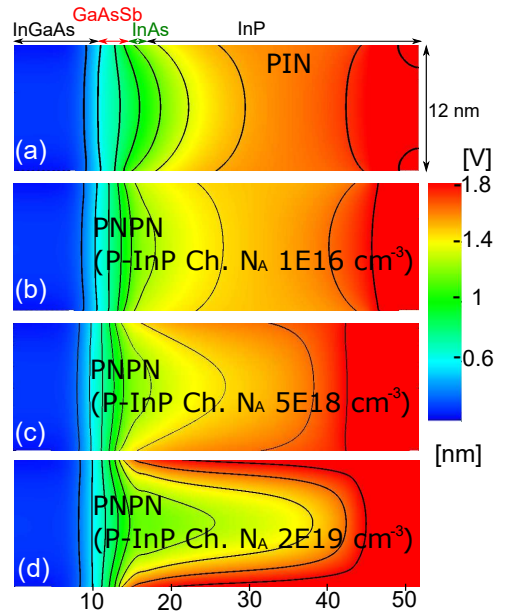
**Fig. 7:** Local density of states of 12 thick THJ-TFET with (a) the PIN doping profile and (b), (c), (d) the PNPN doping profile. The P-InP channel doping density in (b), (c), and (d) are  $1 \times 10^{16}$ ,  $5 \times 10^{18}$ , and  $2 \times 10^{19} \text{ cm}^{-3}$ , respectively. The local density of states is calculated for the ON-state with  $V_{GS} = 0.3 \text{ V}$ .

channel doped to  $5 \times 10^{18} \text{ cm}^{-3}$  shows sub-40 mV/dec S.S. for a limited range of drain current ( $I_{DS}$ ). However, when the P-InP channel doping density further increases to  $2 \times 10^{19} \text{ cm}^{-3}$ , the performance improves significantly. The ON-current of such case reaches  $325 \mu\text{A}/\mu\text{m}$ . It exhibits the S.S. less than 40 mV/dec over four orders of magnitude in the drain current.

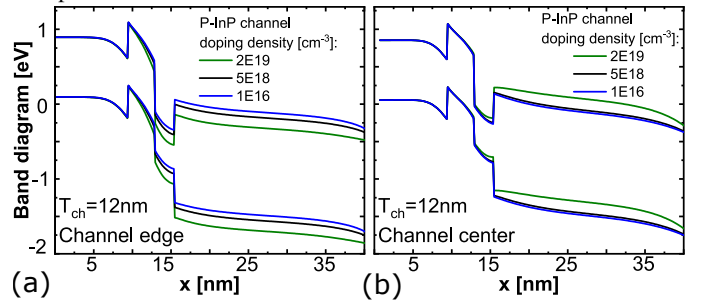
To further understand the impact of P-InP channel doping density, the ON-state local density of state (LDOS) is compared in Fig. 7. In Fig. 7, the LDOS, and the band-diagram are extracted at 1 nm away from the edge of the channel, where the potential is strongly affected by the gate bias. The resonant states in InAs quantum well are outside of the tunneling window in the case of PIN doping profile. On the other hand, for the cases of PNPN-doped THJ-TFET, the resonant states are all located inside the tunneling window regardless of different P-InP channel doping density. This indicates that the improvement when P-InP channel doped to  $2 \times 10^{19} \text{ cm}^{-3}$  comes from other factors other than the alignment of resonant states. The reason is illustrated through the 2D channel potential and the band diagram as shown in Fig. 8 and Fig. 9.

Fig. 8 shows the 2D channel potential for different channel doping profiles. In the case when P-InP channel doped to  $2 \times 10^{19} \text{ cm}^{-3}$ , the 2D channel potential is significantly different from the cases with less channel doping density. The device with such high channel doping density is close to operated in the partially depleted regime; thus, a stronger vertical electric field toward the channel-oxide interface is observed. The strong vertical electric field lowers the channel barrier at the channel edge and increases the tunneling current.

Fig. 9 (a) and (b) show the band diagram at the edge and the center of the channel, respectively. As the channel doping density increases to  $2 \times 10^{19} \text{ cm}^{-3}$ , the valence band at the edge of the channel that close to the channel-oxide interface (depleted region) is further pushed down, which opens up a much lower resistant path comparing to other cases. Although the channel barrier at the center of the channel increases, it does not reduce the current, since the channel center is not



**Fig. 8:** Channel potential of the (a) PIN and (b), (c), (d) PNPN doping profile. The P-InP channel doping density in (b), (c), and (d) are  $1 \times 10^{16} \text{ cm}^{-3}$ ,  $5 \times 10^{18} \text{ cm}^{-3}$ , and  $2 \times 10^{19} \text{ cm}^{-3}$ , respectively. The potentials are obtained for the ON-state with  $V_{GS} = 0.3 \text{ V}$ .



**Fig. 9:** The ON-state band diagram calculated at (a) the edge and (b) the center of the channel.

the main path to conduct the current. As a result, a higher ON-current can be obtained as the channel doping density increases to  $2 \times 10^{19} \text{ cm}^{-3}$ .

## VI. SUMMARY

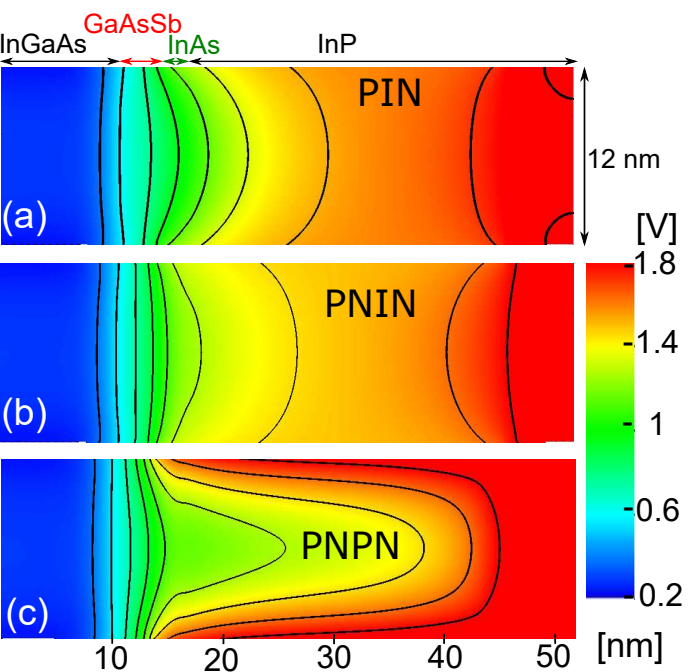
A triple heterojunction TFET design is proposed, considering fabrication constraints such as the channel thickness and the limitation in doping density of the materials. A triple heterojunction TFET with a conventional PIN doping profile is shown to degrade in performance when the body thickness increases from 4 nm to 12 nm. The new doping profile is engineered to increase the electric field in the tunneling junction and reduce the sensitivity of the performance to the body thickness. The ON-current of the optimized design reaches  $325 \mu\text{A}/\mu\text{m}$ , and the S.S. is less than 40 mV/dec over four orders of magnitude in the drain current.

## REFERENCES

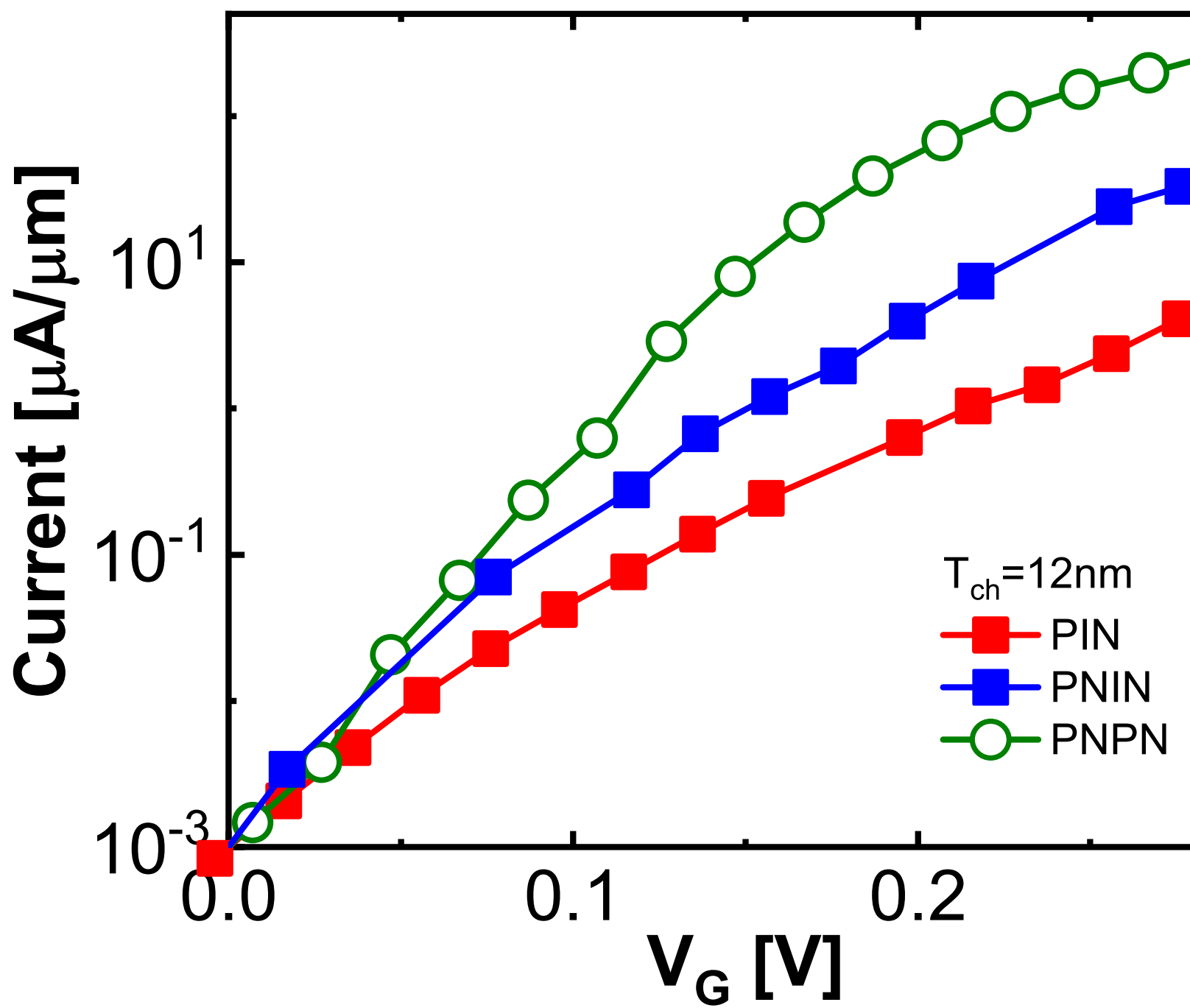
- [1] M. Bohr, "Intel's Revolutionary 22 nm Transistor Technology," [http://download.intel.com/newsroom/kits/22nm/pdfs/22nm-Details\\_Presentation.pdf](http://download.intel.com/newsroom/kits/22nm/pdfs/22nm-Details_Presentation.pdf), 2011. [Online].
- [2] Gonzalez, R. and Gordon, B.M. and Horowitz, M.A., "Supply and threshold voltage scaling for low power CMOS," *IEEE Journal of Solid-State Circuits*, vol. 32, no. 8, pp. 1210–1216, 1997. DOI:10.1109/4.604077.

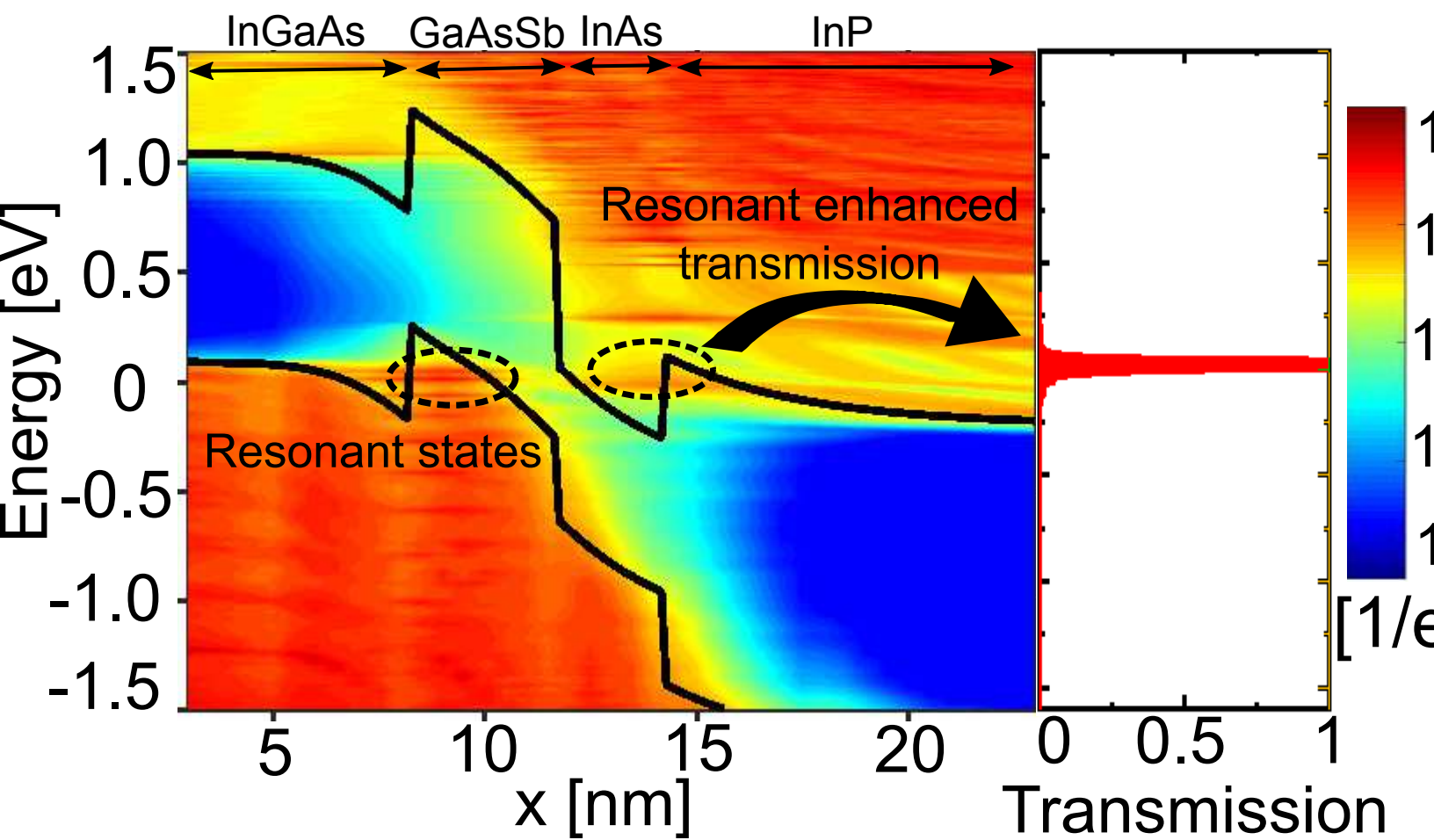
- [3] E. Memisevic, J. Svensson, M. Hellenbrand, E. Lind, and L.-E. Wernersson, "Vertical InAs/GaAsSb/GaSb tunneling field-effect transistor on Si with SS = 48 mV/decade and Ion = 10  $\mu\text{A}/\mu\text{m}$  for Ioff = 1 nA/ $\mu\text{m}$  at Vds = 0.3 V," *2016 IEEE International Electron Devices Meeting (IEDM)*, pp. 19.1.1–19.1.4, 2016. DOI: 10.1109/IEDM.2016.7838450.
- [4] E. Memisevic, J. Svensson, E. Lind, and L. E. Wernersson, "InAs/InGaAsSb/GaSb Nanowire Tunnel Field-Effect Transistors," *IEEE Transactions on Electron Devices*, vol. 64, no. 11, pp. 4746–4751, 2017. DOI:10.1109/TED.2017.2750763.
- [5] E. Memisevic, J. Svensson, E. Lind, and L. E. Wernersson, "Vertical Nanowire TFETs with Channel Diameter Down to 10 nm and Point  $S_{min}$  of 35 mV/Decade," *IEEE Electron Device Letters*, vol. 39, no. 7, pp. 1089–1091, 2018. DOI:10.1109/LED.2018.2836862.
- [6] D. K. Mohata, R. Bijesh, S. Mujumdar, C. Eaton, R. Engel-Herbert, T. Mayer, V. Narayanan, J. M. Fastenau, D. Loubichev, A. K. Liu, and S. Datta, "Demonstration of mosfet-like on-current performance in arsenide/antimonide tunnel fets with staggered hetero-junctions for 300mv logic applications," in *2011 International Electron Devices Meeting*, pp. 33.5.1–33.5.4, Dec 2011. DOI:10.1109/IEDM.2011.6131665.
- [7] S. Sant, K. Moselund, S. Member, D. Cutaita, S. Member, H. Schmid, M. Borg, H. Riel, S. Member, and A. Schenk, "Lateral InAs / Si p-Type Tunnel FETs Integrated on Si. Part 1 : experiment and device," *Ieee Transactions on Electron Devices*, vol. 63, no. 11, pp. 4240–4247, 2016. DOI:10.1109/TED.2016.2612484.
- [8] J. Appenzeller, Y.-M. Lin, J. Knoch, and P. Avouris, "Band-to-band tunneling in carbon nanotube field-effect transistors," *Phys. Rev. Lett.*, vol. 93, p. 196805, Nov 2004. DOI:10.1103/PhysRevLett.93.196805.
- [9] J. Appenzeller, Y. M. Lin, J. Knoch, Z. Chen, and P. Avouris, "Comparing carbon nanotube transistors - the ideal choice: A novel tunneling device design," *IEEE Transactions on Electron Devices*, vol. 52, no. 12, pp. 2568–2576, 2005. DOI:10.1109/TED.2005.859654.
- [10] A. M. Ionescu and H. Riel, "Tunnel field-effect transistors as energy-efficient electronic switches," *Nature*, vol. 479, no. 7373, pp. 329–337, 2011. DOI:10.1038/nature10679.
- [11] U. E. Avci, D. H. Morris, and I. a. Young, "Tunnel field-effect transistors: Prospects and challenges," *IEEE Journal of the Electron Devices Society*, vol. 3, no. 3, pp. 88–95, 2015. DOI:10.1109/JEDS.2015.2390591.
- [12] C.-S. Pang, C.-Y. Chen, T. Ameen, S. Zhang, H. Ilatikhameneh, R. Rahman, G. Klimeck, and Z. Chen, "Wse2 homojunction devices: Electrostatically configurable as diodes, mosfets, and tunnel fets for reconfigurable computing," *Small*, vol. 15, no. 41, p. 1902770, 2019. DOI:10.1002/smll.201902770.
- [13] A. I. Khan, C. W. Yeung, Chenming Hu, and S. Salahuddin, "Ferroelectric negative capacitance mosfet: Capacitance tuning antiferroelectric operation," in *2011 International Electron Devices Meeting*, pp. 11.3.1–11.3.4, Dec 2011. DOI:10.1109/IEDM.2011.6131532.
- [14] K. S. Li, P. G. Chen, T. Y. Lai, C. H. Lin, C. C. Cheng, C. C. Chen, Y. J. Wei, Y. F. Hou, M. H. Liao, M. H. Lee, M. C. Chen, J. M. Sheih, W. K. Yeh, F. L. Yang, S. Salahuddin, and C. Hu, "Sub-60mV-swing negative-capacitance FinFET without hysteresis," *Technical Digest - International Electron Devices Meeting, IEDM*, vol. 2016-February, no. December, pp. 22.6.1–22.6.4, 2015. DOI:10.1109/IEDM.2015.7409760.
- [15] Seabaugh, Alan C. and Zhang, Qin, "Low-voltage tunnel transistors for beyond CMOS logic," *Proceedings of the IEEE*, vol. 98, no. 12, pp. 2095–2110, 2010. DOI:10.1109/JPROC.2010.2070470.
- [16] T. A. Ameen, H. Ilatikhameneh, P. Fay, A. Seabaugh, R. Rahman, and G. Klimeck, "Alloy engineered nitride tunneling field-effect transistor: A solution for the challenge of heterojunction tfets," *IEEE Transactions on Electron Devices*, vol. 66, pp. 736–742, Jan 2019. DOI:10.1109/TED.2018.2877753.
- [17] Ilatikhameneh, Hesameddin and Ameen, Tarek a. and Klimeck, Gerhard and Appenzeller, Joerg and Rahman, Rajib, "Dielectric Engineered Tunnel Field-Effect Transistor," *IEEE Electron Device Letters*, vol. 36, no. 10, pp. 1097–1100, 2015. DOI:10.1109/LED.2015.2474147.
- [18] U. E. Avci and I. A. Young, "Heterojunction TFET Scaling and resonant-TFET for steep subthreshold slope at sub-9nm gate-length," in *2013 IEEE International Electron Devices Meeting*, pp. 4.3.1–4.3.4, Dec 2013. DOI:10.1109/IEDM.2013.6724559.
- [19] T. A. Ameen, H. Ilatikhameneh, G. Klimeck, and R. Rahman, "Few-layer phosphorene: An ideal 2D material for tunnel transistors," *Scientific Reports*, vol. 6, no. June, pp. 1–7, 2016. DOI:10.1038/srep28515.
- [20] J. Z. Huang, P. Long, M. Povolotskyi, G. Klimeck, and M. J. Rodwell, "P-Type Tunnel FETs with Triple Heterojunctions," *IEEE Journal of the Electron Devices Society*, vol. 4, no. 6, pp. 410–415, 2016. DOI:10.1109/JEDS.2016.2614915.
- [21] P. Long, J. Z. Huang, M. Povolotskyi, D. Verreck, G. Klimeck, and M. J. W. Rodwell, "High-current inp-based triple heterojunction tunnel transistors," in *2016 Compound Semiconductor Week (CSW) [Includes 28th International Conference on Indium Phosphide Related Materials (IPRM) 43rd International Symposium on Compound Semiconductors (ISCS)*, pp. 1–2, June 2016. DOI:10.1109/ICIPRM.2016.7528592.
- [22] Long, Pengyu and Povolotskyi, Michael and Huang, Jun Z. and Charles, James and Kubis, Tillmann and Klimeck, Gerhard and Rodwell, Mark J.W., "A high-current InP-channel triple heterojunction tunnel transistor design," *Device Research Conference - Conference Digest, DRC*, no. June, pp. 10–12, 2017. DOI:10.1109/DRC.2017.7999437.
- [23] Jun Z. Huang, Pengyu Long, Michael Povolotskyi, Gerhard Klimeck, Mark J.W. Rodwell, "Sb- and Al- free ultra-high-current tunnel FET design," *2017 Fifth Berkeley Symposium on Energy Efficient Electronic Systems & Steep Transistors Workshop (E3S)*, no. IEEE, pp. 8–10, 2017. DOI:10.1109/E3S.2017.8246174.
- [24] H. Ilatikhameneh, T. A. Ameen, C. Chen, G. Klimeck, and R. Rahman, "Sensitivity challenge of steep transistors," *IEEE Transactions on Electron Devices*, vol. 65, no. 4, pp. 1633–1639, 2018. DOI: 10.1109/TED.2018.2808040.
- [25] C. Chen, T. A. Ameen, H. Ilatikhameneh, R. Rahman, G. Klimeck, and J. Appenzeller, "Channel thickness optimization for ultrathin and 2-d chemically doped tfets," *IEEE Transactions on Electron Devices*, vol. 65, pp. 4614–4621, Oct 2018. DOI:10.1109/TED.2018.2862408.
- [26] S. Steiger, M. Povolotskyi, H. H. Park, T. Kubis, and G. Klimeck, "NEMO5: A parallel multiscale nanoelectronics modeling tool," *IEEE Transactions on Nanotechnology*, vol. 10, no. 6, pp. 1464–1474, 2011. DOI:10.1109/TNANO.2011.2166164.
- [27] J. E. Fonseca, T. Kubis, M. Povolotskyi, B. Novakovic, a. Ajoy, G. Hegde, H. Ilatikhameneh, Z. Jiang, P. Sengupta, Y. Tan, and G. Klimeck, "Efficient and realistic device modeling from atomic detail to the nanoscale," *Journal of Computational Electronics*, vol. 12, no. 4, pp. 592–600, 2013.
- [28] Y. Tan, M. Povolotskyi, T. Kubis, T. B. Boykin, and G. Klimeck, "Transferable tight-binding model for strained group IV and III-V materials and heterostructures," *Physical Review B*, vol. 94, no. 4, pp. 1–17, 2016. DOI:10.1103/PhysRevB.94.045311.
- [29] M. Luisier and G. Klimeck, "Atomistic full-band simulations of silicon nanowire transistors: Effects of electron-phonon scattering," *Physical Review B - Condensed Matter and Materials Physics*, vol. 80, no. 15, pp. 1–11, 2009. DOI:10.1103/PhysRevB.80.155430.
- [30] R. Lake, G. Klimeck, R. C. Bowen, and D. Jovanovic, "Single and multiband modeling of quantum electron transport through layered semiconductor devices," *Journal of Applied Physics*, vol. 81, no. 12, pp. 7845–7869, 1997. DOI:10.1063/1.365394.
- [31] J. Geng, P. Sarangapani, K.-C. Wang, E. Nelson, B. Browne, C. Wordelman, J. Charles, Y. Chu, T. Kubis, and G. Klimeck, "Quantitative multiscale, multi-physics quantum transport modeling of gan-based light emitting diodes," *physica status solidi (a)*, vol. 215, no. 9, p. 1700662, 2018. DOI:10.1002/psa.201700662.
- [32] Y. Hsueh, A. Tankasala, Y. Wang, G. Klimeck, M. Simmons, and R. Rahman, "Phonon induced two-electron relaxation in two donor qubits in silicon," in *APS March Meeting Abstracts*, 2016.
- [33] J. Salfi, B. Voisin, A. Tankasala, J. Bocquel, M. Usman, M. Simmons, L. Hollenberg, R. Rahman, and S. Rogge, "Valley filtering in spatial maps of coupling between silicon donors and quantum dots," *Physical Review X*, vol. 8, no. 3, p. 031049, 2018. DOI:10.1103/PhysRevX.8.031049.
- [34] A. Tankasala, J. Salfi, J. Bocquel, B. Voisin, M. Usman, G. Klimeck, M. Y. Simmons, L. C. Hollenberg, S. Rogge, and R. Rahman, "Two-electron states of a group-V donor in silicon from atomistic full configuration interactions," *Physical Review B*, vol. 97, no. 19, p. 195301, 2018. DOI:10.1103/PhysRevB.97.195301.
- [35] A. Tankasala, Y. Wang, G. Klimeck, and R. Rahman, "Atomistic configuration interaction simulations of two-electron states of donors in silicon," in *APS Meeting Abstracts*, 2015.
- [36] F. Mazzola, C.-Y. Chen, R. Rahman, X.-G. Zhu, C. M. Polley, T. Balasubramanian, P. D. C. King, P. Hofmann, J. A. Miwa, and J. W. Wells, "The sub-band structure of atomically sharp dopant profiles in silicon," *npj Quantum Materials*, vol. 5, p. 34, Jun 2020. DOI:10.1038/s41535-020-0237-1.
- [37] J. Z. Huang, P. Long, M. Povolotskyi, H. Ilatikhameneh, T. a. Ameen, R. Rahman, M. J. Rodwell, and G. Klimeck, "A Multiscale Modeling of Triple-Heterojunction Tunneling FETs," *IEEE Transactions on Electron Devices*, vol. 64, no. 6, pp. 2728–2735, 2017. DOI:10.1109/TED.2017.2690669.
- [38] T. A. Ameen, H. Ilatikhameneh, J. Z. Huang, M. Povolotskyi, R. Rahman, and G. Klimeck, "Combination of Equilibrium and Nonequilibrium Carrier Statistics into an Atomistic Quantum Transport Model for

- Tunneling Heterojunctions,” *IEEE Transactions on Electron Devices*, vol. 64, no. 6, pp. 2512–2518, 2017. DOI:10.1109/TED.2017.2690626.
- [39] C. Chen, H. Ilatikhameneh, J. Z. Huang, G. Klimeck, and M. Povolotskiy, “Impact of Body Thickness and Scattering on III–V Triple Heterojunction TFET Modeled With Atomistic Mode-Space Approximation,” *IEEE Transactions on Electron Devices*, vol. 67, no. 8, pp. 3478–3485, 2020. DOI: 10.1109/TED.2020.3002220.
- [40] M. Fujimatsu, H. Saito, and Y. Miyamoto, “71 mv/dec of sub-threshold slope in vertical tunnel field-effect transistors with GaSb/InGaAs heterostructure,” in *2012 International Conference on Indium Phosphide and Related Materials*, pp. 25–28, Aug 2012. DOI:10.1109/ICIPRM.2012.6403309.
- [41] A. Tabata, T. Benyattou, G. Guillot, Z. Sobiesierski, S. A. Clark, R. H. Williams, M. Gendry, G. Hollinger, and P. Viktorovitch, “Surface InAs/InP quantum wells: epitaxial growth and characterization,” in *[Proceedings 1991] Third International Conference Indium Phosphide and Related Materials*, pp. 496–499, April 1991. DOI:10.1109/ICIPRM.1991.147421.
- [42] Gan Feng and Kunishige Oe and Masahiro Yoshimoto, “Temperature dependence of Bi behavior in MBE growth of InGaAs/InP,” *Journal of Crystal Growth*, vol. 301-302, pp. 121 – 124, 2007. 14th International Conference on Molecular Beam Epitaxy, DOI:https://doi.org/10.1016/j.jcrysgro.2006.11.242.
- [43] B. Lambert, Y. Toudic, Y. Rouillard, M. Gauneau, M. Baudet, F. Alard, I. Valiente, and J. C. Simon, “High reflectivity 1.55  $\mu\text{m}$  (Al)GaAsSb/AlAsSb Bragg reflector lattice matched on InP substrates,” *Applied Physics Letters*, vol. 66, no. 4, pp. 442–444, 1995. DOI:10.1063/1.114050.
- [44] J. W. Matthews and A. E. Blakeslee, “Defects in epitaxial multilayers. I. Misfit dislocations,” *Journal of Crystal Growth*, vol. 27, pp. 118–125, dec 1974. DOI:10.1016/0022-0248(74)90424-2.
- [45] T. Akazaki, K. Arai, T. Enoki, and Y. Ishii, “Improved InAlAs/InGaAs HEMT characteristics by inserting an InAs layer into the InGaAs channel,” *IEEE Electron Device Letters*, vol. 13, no. 6, pp. 325–327, 1992. DOI:10.1109/55.145073.
- [46] V. Nagavarapu, R. Jhaveri, and J. C. Woo, “The tunnel source (PNPN) n-MOSFET: A novel high performance transistor,” *IEEE Transactions on Electron Devices*, vol. 55, no. 4, pp. 1013–1019, 2008. DOI:10.1109/TED.2008.916711.
- [47] D. B. Abdi and M. J. Kumar, “In-built N+ Pocket p-n-p-n tunnel field-effect transistor,” *IEEE Electron Device Letters*, vol. 35, no. 12, pp. 1170–1172, 2014. DOI:10.1109/LED.2014.2362926.
- [48] S. Baronia, K. Nigam, D. Sharma, B. R. Raad, and P. Kondekar, “A novel approach of PNP dual metal double gate tunnel field effect transistor for improving DC characteristics,” *Proceedings of 2016 International Conference on Advanced Communication Control and Computing Technologies, ICACCCT 2016*, no. 978, pp. 44–47, 2017.
- [49] D. B. Abdi and M. J. Kumar, “2-D Threshold Voltage Model for the Double-Gate p-n-p-n TFET With Localized Charges,” *IEEE Transactions on Electron Devices*, vol. 63, pp. 3663–3668, Sep. 2016. DOI:10.1109/TED.2016.2589927.
- [50] H. Ilatikhameneh, G. Klimeck, J. Appenzeller, and R. Rahman, “Scaling Theory of Electrically Doped 2D Transistors,” *IEEE Electron Device Letters*, vol. 36, no. 7, pp. 726–728, 2015. DOI:10.1109/LED.2015.2436356.
- [51] H. Ilatikhameneh, R. B. Salazar, G. Klimeck, R. Rahman, and J. Appenzeller, “From fowler–nordheim to nonequilibrium green’s function modeling of tunneling,” *IEEE Transactions on Electron Devices*, vol. 63, pp. 2871–2878, July 2016. DOI:10.1109/TED.2016.2565582.









This figure "universe.jpg" is available in "jpg" format from:

<http://arxiv.org/ps/2010.12964v1>